2007

The use of a chiral fluorescent resorcinarene for the enantiomeric recognition of amino acids

Gerald I. Richard
Louisiana State University and Agricultural and Mechanical College, gricha9@lsu.edu

THE USE OF A CHIRAL FLUORESCENT RESORCINARENE FOR THE ENANTIOMERIC RECOGNITION OF AMINO ACIDS

A Thesis

Submitted to the Graduate Faculty of the
Louisiana State University and
Agricultural and Mechanical College
in partial fulfillment of the
requirements for the degree of
Master of Science

in

The Department of Chemistry

by
Gerald I. Richard
B.S., Xavier University of Louisiana, 2002
December 2007

ACKNOWLEDGEMENTS

I would like to extend appreciation to my research advisor, Dr. Isiah Warner, for affording me the opportunity to work in his research group and for all of his support and patience. I would also like to extend my appreciation to Dr. Robert Strongin and his research group, especially Shan Jiang, for their help with my research. To all of the current and former post-docs and members of the Warner research group, particularly Hadi Marwani, Alicia Williams, Vivian Fernand, Gabriela Ganea, Arther Gates, Dr. Sayo Fakayode, and Dr. Mark Lowry, thank you. I also want to thank my committee members, Dr. Michael Tolocka and Dr. Steven Watkins. Lastly, I thank my family for their support and encouragement. Special thanks to the National Science Foundation, National Institutes of Health, and Louisiana State University for financial support during my graduate career.

TABLE OF CONTENTS

LIST OF TABLES

LIST OF FIGURES

ABSTRACT

The spectroscopic properties of a chiral boronic acid based resorcinarene macrocycle employed for chiral analysis were investigated. Specifically, the emission and excitation characteristics of tetraarylboronate resorcinarene macrocycle (TBRM) and its quantum yield were evaluated. The chiral selector TBRM was investigated as a chiral reagent for the enantiomeric discrimination of amino acids using steady-state fluorescence spectroscopy. Chiral recognition of amino acids in the presence of the macrocycle was based on diastereomeric complexes. Results demonstrated that TBRM had better chiral discrimination ability for lysine as compared to the other amino acids. Partial-least-squares regression modeling (PLS-1) of spectral data for macrocycle-lysine host-guest complexes was used to correlate the changes in the fluorescence emission for a set of calibration samples consisting of TBRM in the presence of varying enantiomeric compositions of lysine. In addition, validation studies were performed using an independently prepared set of samples with different enantiomeric compositions of lysine. The results of multivariate regression modeling indicated good prediction ability of lysine which was confirmed by a root-mean-square percent relative error (*RMS%RE*) of 5.8 %.

CHAPTER 1

INTRODUCTION

1.1 Chirality

Chirality is the structural property of an object or molecule which is nonsuperimposable with its mirror image [1]. Moreover, a chiral molecule is one that is not identical with its mirror image. The word chiral is derived from the Greek word *cheir* which means hand. The human hands are the most well-known and easily observable example of chirality. When viewed in a mirror, the left hand is the mirror image of the right hand, and the hands are not identical or superimposable. Therefore, the hands are enantiomers or chiral.

In 1848, Louis Pasteur's separation of sodium ammonium tartrate crystals of tartaric acid led to the discovery of chirality. During his initial investigation of the crystals, Pasteur noticed that there were two forms of the crystals present, and they were mirror images of each other. He meticulously separated the two forms by hand using tweezers and a magnifying glass. Solutions of each crystal form were placed in a polarimeter, and Pasteur observed that the solutions rotated polarized light in opposite directions and with an equal magnitude. However, an equal mixture of the two solutions resulted in no rotation of the polarized light. Therefore, Pasteur concluded that the observed differences in optical activity were due to the differences in chirality of the crystals [2].

1.1.1 Nomenclature of Chiral Molecules

Enantiomers are chiral molecules as well as optical isomers that are not identical with their mirror images. They are optically active molecules and differ in the direction in which they rotate plane polarized light. Enantiomers can be named by the direction that plane polarized light is rotated. If an enantiomer rotates light in a clockwise direction, then it is called dextrorotatory (*d*) and is labeled with a positive (+) sign. Whereas, an enantiomer which rotates

light in a counterclockwise direction is called levorotatory (*l*) and is labeled with a negative (-) sign. Dextrorotatory and levorotatory are from the Latin words *dexter* and *laevus*, meaning right and left, respectively.

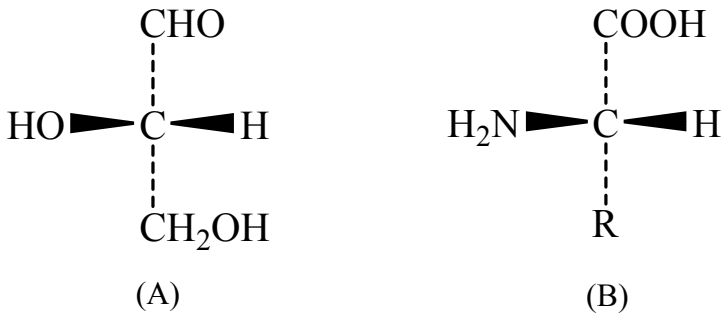

Figure 1.1 Chemical structures of (A) L-glyceraldhyde and (B) L-amino acid.

Chiral molecules can also be named by the D-L system which is based on an enantiomer's stereochemical configuration relative to the carbohydrate glyceraldehyde. In other words, the spatial configuration of atoms around any chiral center can be related to glyceraldehyde by converting the atoms to that of D- or L-glyceraldehyde. This system was devised by Emil Fischer in 1891, and it is generally used for naming amino acid and carbohydrate enantiomers. As illustrated in Figure 1.1, the amino, carboxyl, side chain (R), and hydrogen groups around the alpha-carbon of amino acids correspond to the hydroxyl, aldehyde, CH_2OH, and hydrogen groups of glyceraldehyde, respectively. So, L-amino acids and L-glyceraldehyde have the same relative configuration while D-amino acids and D-glyceraldehyde have the same one. The D- or L- designation of an enantiomer is not necessarily indicative of its ability to rotate plane polarized light. For instance, the carbohydrate D-fructose is levorotatory, and several L-amino acids are dextrorotatory. When Fischer created this system, he arbitrarily labeled the glyceraldehyde enantiomer, which rotated plane polarized light clockwise, as D without knowing

if it was actually dextrorotatory. The other glyceraldehyde enantiomer, which rotated plane polarized light counterclockwise, was labeled as L.

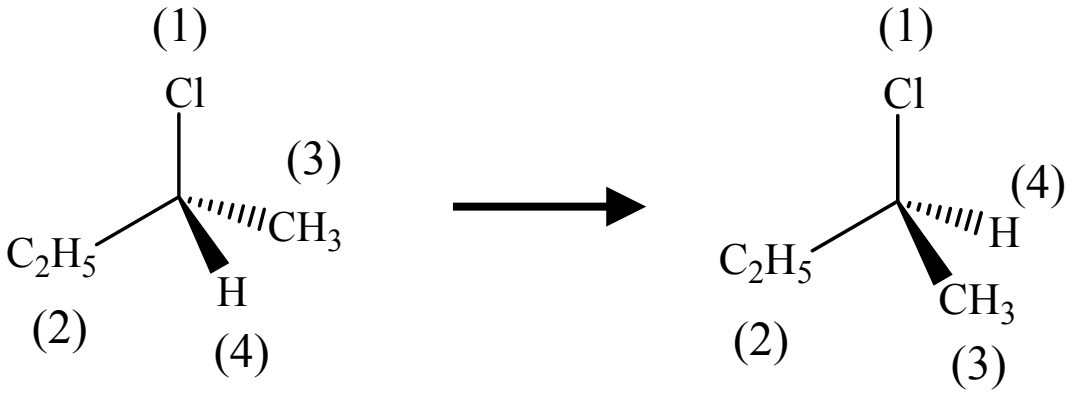

Figure 1.2 An example in determining the R-S configuration of a chiral molecule.

The most commonly and widely used nomenclature for enantiomers is the Cahn-Ingold-Prelog system or better known as the R-S system, which was created in 1956 by Robert Cahn, Christopher Ingold, and Vladimir Prelog. This system can describe the configuration of chiral molecules with one or more chiral centers, and it labels each chiral center according to specific preferences or priority rules. Each substituent connected to the chiral center is assigned a priority based upon atomic number. The highest priority is assigned to the substituent with the highest atomic number whereas the lowest priority is assigned to the substituent with the lowest atomic number. If the substituents directly attached to the chiral center are identical, then the next substituent outward from the chiral center is examined and priority is assigned at the first point of difference. To determine the R-S configuration, the molecule is rotated so that the lowest priority substituent is directed away from the viewer as illustrated in Figure 1.2. If the three higher priority groups decreases in a clockwise direction, then the enantiomer is labeled as *R* or *rectus*. However, if the priority decreases in a counterclockwise direction, then the enantiomer is labeled as *S* or *sinister*. *Rectus* and *sinister* are Latin words for right and left,

respectively. The *R* or *S* designation of an enantiomer is not necessarily correlated with its ability to rotate plane polarized light or with the D-L system. In fact, all L-amino acids except cysteine are (S)-amino acids.

1.1.2 Types of Chirality

There are two major types of chirality—point chirality or axial chirality—in which a chiral molecule can be classified. Point chirality results from molecules which have four different substituents attached to an asymmetric center or chiral center. Usually, the chiral center is a tetrahedral carbon, but any tetrahedral atom such as silicon or germanium, with four different substituents can be a chiral center. Regardless of the number of chiral centers, a molecule is not chiral if is possesses a plane of symmetry. Molecules with a plane of symmetry are called achiral.

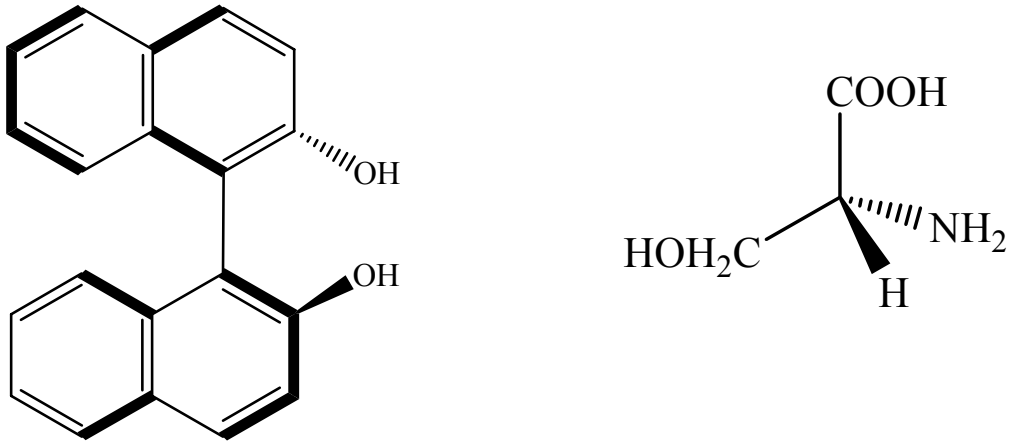

Figure 1.3 Chemical structures of axial chiral and point chiral molecules.

While point chirality is the most common type of chirality, many chiral molecules possess axial chirality. Axial chirality results from molecules which do not possess a chiral center but do

possess an asymmetric plane. In other words, chirality occurs when the rotation about a central bond is restricted and substituents are held in a nonsuperimposable spatial arrangement. For example, biphenyls and binapthols have axial chirality. Figure 1.3 illustrates examples of point and axial chirality.

1.1.3 Significance of Chirality

In an achiral environment, enantiomers have identical properties such as boiling point, melting point, solubility, refractive index, density, and reaction rate. Moreover, the intermolecular forces of both enantiomers are identical as well. On the other hand, enantiomers behave differently in a chiral environment. For instance, enantiomers have different solubilites when dissolved in the same chiral solvent, and they have different reaction rates when reacted with the same chiral reagent.

Chirality has an important influence on biological systems such as plants and animals. Most biological molecules, i.e. DNA, proteins, enzymes, amino acids, and carbohydrates, are chiral [3-8]. However, only one enantiomeric form is usually present in a particular species. For humans, amino acids exclusively exist as L enantiomers whereas carbohydrates only exist as D enantiomers. Even though they are equally stable as their respective counterparts, L-amino acids and D-carbohydrates are the naturally favored enantiomers. Specifically, proteins composed of L-amino acids will react with a certain L-amino acid but will not readily react with the D form of the same amino acid. However, the presence of D-amino acids at low levels has been reported in humans, and they may have an antagonistic biological function [9-11].

Enantiomers can have different effects on humans in the form of smell, taste, or physiological activity [12]. Because human odor receptors are chiral, humans are able to recognize that (R)-limonene smells like lemons and (S)-limonene smells like oranges. Likewise, D-asparagine tastes sweet and L-asparagine tastes bitter because human taste receptors are chiral.

In addition, chiral drugs can have a profound effect on human physiological activity. While one enantiomer of a chiral drug may be physiologically active, the other enantiomer may be physiologically inactive or even toxic [13, 14]. For example, only the (S)-enantiomer of ibuprofen is effective as an anti-inflammatory agent whereas the (R)-enantiomer has no physiological activity. Furthermore, the significance of chirality was demonstrated by the effects of the thalidomide tragedy [15]. Sold as a racemic mixture in the early 1960s, thalidomide was prescribed to pregnant women to alleviate morning sickness. It was later discovered as the cause of horrible birth defects in several children. Eventually, the (R)-enantiomer of thalidomide was determined as the therapeutic agent which relieved morning sickness while the (S)-enantiomer was identified as the toxic agent which prevented normal fetus growth and development, resulting in birth defects. Moreover, the thalidomide enantiomers are racemized and interconverted in the human body.

1.1.4 Methods of Chiral Analysis

Since the thalidomide tragedy, the development of analytical methods for chiral analysis has become an important focus for industries such as the pharmaceutical and agricultural industries. In fact, the Food and Drug Administration requires that chiral drugs, which are sold as single enantiomers, undergo strict pharmacological and physiological testing [16]. The effects of both enantiomers are established, and the enantiomeric purity of the chiral drugs is determined before being placed on the market. Presently, there are several analytical techniques used to investigate chiral molecules. These techniques are based upon chromatographic or spectroscopic methods. The chromatographic methods involve gas chromatography (GC) [17, 18], high performance liquid chromatography (HPLC) [19, 20], and capillary electrophoresis (CE) [21, 22]. The spectroscopic methods include nuclear magnetic resonance (NMR) [23, 24], mass spectrometry (MS) [25, 26], circular dichroism (CD) [27], ultraviolet-visible spectroscopy

(UV-vis) [28], and fluorescence spectroscopy [29, 30]. While these methods are effective for chiral analysis, they all have certain limitations. All of the chromatographic methods involve relatively long analysis times. GC requires volatile analytes while HPLC consumes large volumes of both reagents and analytes. On the other hand, MS can be destructive for the analyte. NMR requires somewhat expensive chiral reagents and lacks in sensitivity. CD and UV-vis are limited by the use of a chromophore, and CD is relatively not as sensitive. However, the use of fluorescence spectroscopy for enantioselective discrimination offers several advantages such as relatively high sensitivity, selectivity, and versatility. Although fluorescence spectroscopy can be a very advantageous method, it is limited by the use of a fluorophore. Fluorescence spectroscopy will be discussed further in a later section.

1.1.5 Chiral Selectors

A chiral selector is a chiral molecule which differentiates between two enantiomers of the same molecule. The enantioselectivity of a chiral selector depends on its more favorable interaction with one enantiomer over the other one. Some commonly used chiral selectors include cyclodextrins, crown ethers, molecular micelles, and resorcinarenes [31-34]. Since a resorcinarene based chiral selector was used for the studies in this thesis, further discussion will be limited to resorcinarenes.

Resorcinarenes, which are a class of calixarenes, are cyclic aromatic tetramers synthesized in a single step from an acid catalyzed condensation reaction of resorcinol and an aldehyde [35]. Resorcinarenes are macrocyclic molecules composed of phenolic units linked by methylene bridges. In 1872, Adolf von Baeyer first discovered resorcinarenes while developing phenol based dyes [36, 37]. He reported that a mixture of benzaldehyde and resorcinol in the presence of sulfuric acid resulted in a red colored product, which turned violet in basic solution. A crystalline product was formed when the mixture was heated, and it was later established as an

isomer of the red colored product. Baeyer was not able to propose structures of these products due to the limitations of characterization methods at that time. Nevertheless, the elemental composition of the crystalline product $(C_{13}H_{10}O_2)_n$ was determined by Michaelis in 1883. He stated that the product resulted from reacting equal amounts of benzaldehyde and resorcinol as well as the loss of equal amounts of water molecules. In 1940, Niederl and Vogel proposed that the product was a cyclic tetramer, which was structurally similar to porphyrins [38]. Using X-ray analysis, Erdtman finally determined the structure in 1968 [39].

Characterized by a wide upper rim and a relatively narrow lower rim, resorcinarenes have found several applications in material science, molecular recognition, and supramolecular chemistry [35, 40-44]. Many studies have used resorcinarenes for chemical sensing, drug delivery, and catalysis. Typically for these studies, resorcinarenes are prepared by the condensation of resorcinol and an aldehyde in a concentrated acid solution. The upper rim consists of eight phenolic hydroxyl groups which are capable of hydrogen bonding while the lower rim includes four groups which are components of the starting aldehyde material.

1.1.6 Three Point Interaction Model

For chiral discrimination to occur, the formation of diastereomeric complexes between enantiomers and a chiral selector is imperative. Chiral discrimination results from the differences between the two diastereomeric enantiomer-chiral selector complexes as illustrated in Figure 1.4. Details about the mechanism of chiral recognition are not understood very well. Although several chiral discrimination mechanisms have been proposed, the three point interaction model is generally the most accepted one [45, 46]. Proposed by Easson and Stedman, this model states that a minimum of three simultaneous and spatially significant interactions between one enantiomer and chiral selector must exist for chiral discrimination [47]. Because of spatial restraints, no more than two interactions can occur between the other enantiomer and

chiral selector. The interactions between enantiomers and a chiral selector are not necessarily points of molecular attachment. In fact, repulsive forces and steric interactions also aid in chiral discrimination. Other types of interactions include hydrogen bonding, dipole, π- π, hydrophobic, and van der Waals.

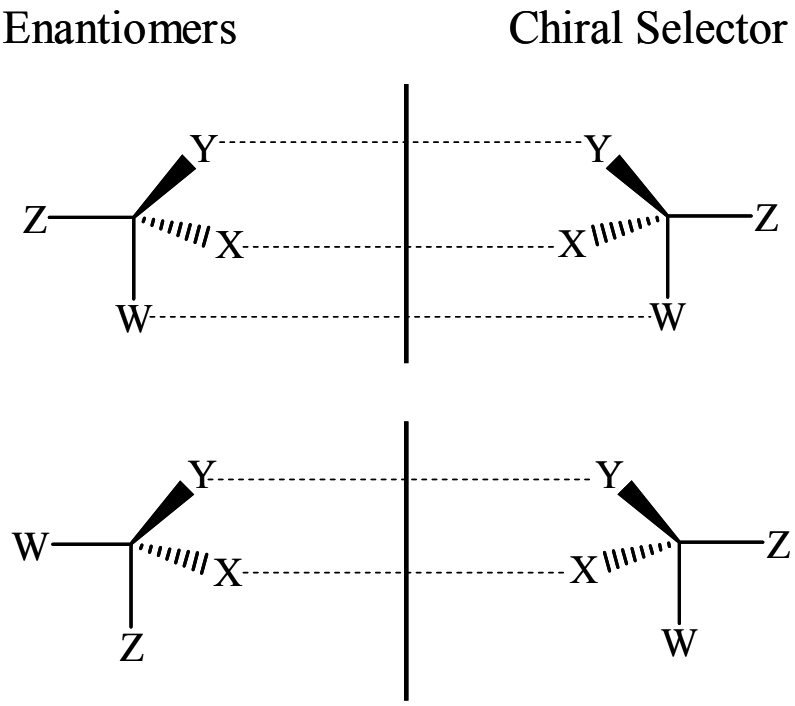

Figure 1.4 Three point interaction model for chiral recognition.

1.2 Fluorescence Spectroscopy

Luminescence is the emission of light as a result of a radiative transition in which a molecule decreases its energy by emission of a photon [48]. The different types of luminescence, i.e. chemiluminescence, photoluminescence, and radioluminescence, are characterized by the source of energy which is used to excite the luminescing molecule. For photoluminescence, the excitation energy results from absorbed photons, but the energy from a chemical reaction supplies the excitation energy for chemiluminescence. Fluorescence is a type of photoluminescence, and it is broadly defined as the radiative emission of light resulting from

the transition of a molecule within the same multiplicity. For most organic molecules, fluorescence occurs from the first excited singlet state (S_1) to the ground singlet state (S_0). A Jablonski energy level diagram (Figure 1.5) provides the best approach to understanding the processes associated with luminescence phenomena such as fluorescence [48]. The ground singlet, first singlet, second singlet, and first triplet electronic states are represented by the thicker horizontal lines labeled S_0, S_1, S_2, and T_1, respectively. The vibrational levels within each electronic state are labeled as v_0, v_1, v_2, and v_3, and they are represented by the thinner horizontal lines.

1.2.1 Theory

At room temperature, most molecules are located in the lowest vibrational level of the ground singlet state because thermal energy is inadequate to populate higher vibrational levels of the ground singlet state. Thus, absorption generally involves the excitation of a molecule from the lowest vibrational level of the ground singlet state. When absorbing photons of light, a molecule is excited to a higher energy state, which can be any of several vibrational levels in the excited singlet states. The absorption process can be described by the Beer-Lambert law, that is,

$$A = \varepsilon bc \tag{1.1}$$

where A is the absorbance of a molecule, ε is the molar absorptivity, b is the cell pathlength, and c is the molar concentration of the molecule. In other words, the absorbance is the product of the molar absorpitivity, cell pathlength, and molar concentration. The absorbance can also be expressed as a logarithmic ratio of the incident light and transmitted light, as given by

$$A = \log \frac{I_o}{I_t} \tag{1.2}$$

where I_o is the intensity of the incident light and I_t is the intensity of the transmitted light.

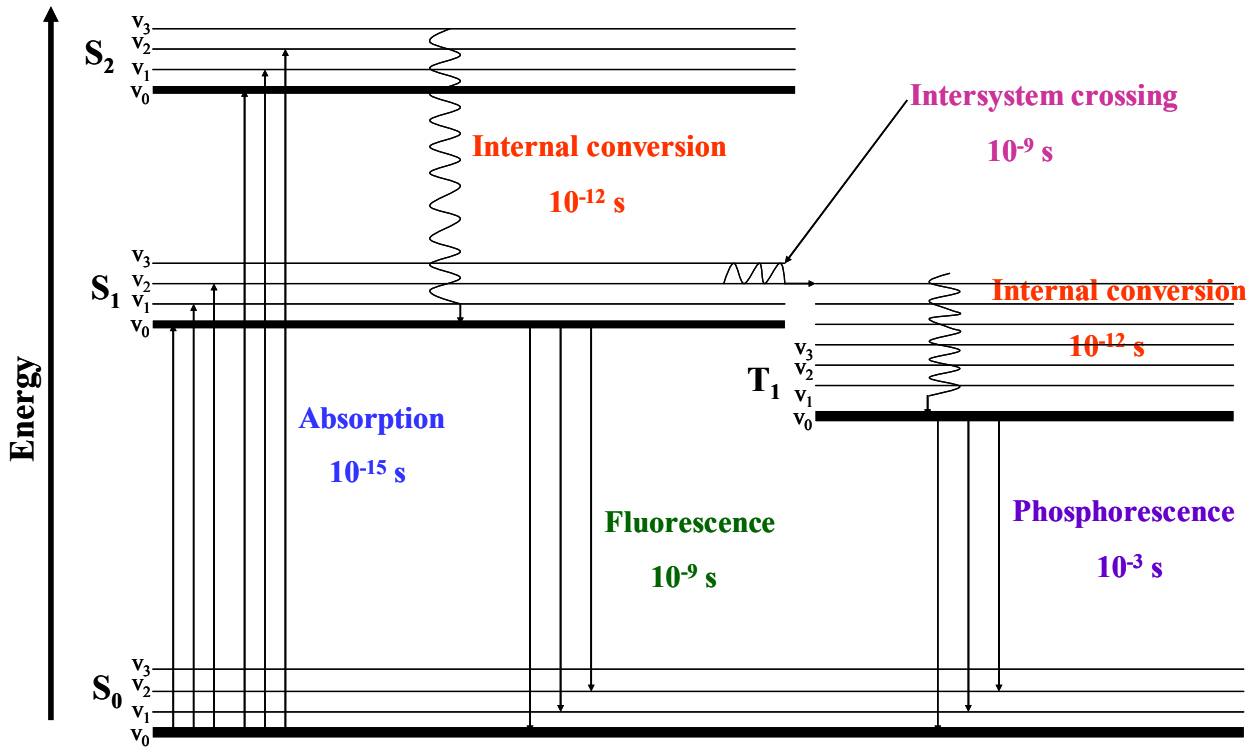

Figure 1.5 Jablonski energy diagram.

Because absorption is an exponential function of the cell pathlength and concentration of the molecule, the absorbance signal measurement is the result of the logarithmic difference of the incident and transmitted intensitites. This is shown by the following equation

$$A = \log I_o - \log I_t \tag{1.3}$$

The absorption process typically occurs within 10^{-15} seconds. After light is absorbed, several radiative and nonradiative processes can occur before a molecule returns to the ground state. The radiative processes are phosphorescence and fluorescence while the nonradiative processes typically include vibrational relaxation, internal conversion, and intersystem crossing.

In an effort to relax to the lowest vibrational level of its excited electronic state, a molecule undergoes vibrational relaxation once it is in the excited state. During this nonradiative

deactivation process, excess vibrational energy is dissipated as heat through collisions with the excited molecule and solvent molecules or other molecules in the excited state. As a result, slight increases in temperature of the excited molecule's surroundings occur after the energy transfer. Generally, vibrational relaxation occurs in 10^{-12} seconds.

Moreover, when a molecule in the excited electronic state transitions to a lower excited electronic state, it undergoes internal conversion. The molecule will relax to the lowest vibrational level of the first excited electronic state. This nonradiative deactivation process is favorable since the energy transitions occur between states of the same multiplicity. Internal conversion also occurs in 10^{-12} seconds. However, internal conversion from the first excited state to the ground state is relatively a slower process.

In addition, a molecule can undergo intersystem crossing while in the excited state. During this nonradiative deactivation process, the molecule transfers energy from the excited singlet state to the excited triplet state. The probability of intersystem crossing occurring is low since it involves changes in multiplicities, which are forbidden processes. However, when intersystem crossing does occur, it is relatively a slower process than internal conversion, and it generally occurs in molecules containing heavy atoms such as bromine and in paramagnetic species such as molecular oxygen. Intersystem crossing typically occurs in 10^{-9} seconds.

After a molecule has transitioned to the excited triplet state, it will relax to the lowest vibrational level of the first excited triplet state. From there, the molecule returns to the ground state by emission of a photon. Phosphorescence is the radiative emission of light resulting from the transition of molecule between states of different multiplicities. As shown in the Jablonski energy diagram, this radiative transition occurs from the first excited triplet state to the ground state. Since the first excited triplet state is lower in energy than the first excited singlet state,

phosphorescence occurs at longer wavelengths than fluorescence. Typically, phosphorescence occurs from 10^{-6} to several seconds.

In contrast, when a molecule has reached the lowest vibrational level of the first excited singlet state, it undergoes fluorescence as it transitions from the first excited singlet state to the ground state. Fluorescence is the radiative emission of light resulting from the transition of a molecule within the same multiplicity. Only for a few molecules, fluorescence emission involves transitions from higher excited singlet states other than the first excited singlet state. Fluorescence generally occurs in 10^{-9} seconds.

1.2.2 Characteristics

In general, there are two characteristics displayed by most fluorescing molecules. Fluorescence (emission) always occurs at longer wavelengths or lower energies than absorption (excitation). This phenomenon is known as Stokes' shift (Figure 1.6) which is the difference in wavelength between the absorption and emission maxima, as show by the equation

$$Stokes'\ shift = 10^7 x\left(\frac{1}{\lambda_{ex}} - \frac{1}{\lambda_{em}}\right) \tag{1.4}$$

where λ_{ex} and λ_{em} are the maximum excitation and maximum emission wavelengths expressed in nanometers [49]. When a molecule is in the excited state, some loss of energy occurs before fluorescence. Therefore, Stokes' shift is the result of energy differences due to the rapid deactivation processes of vibrational relaxation and internal conversion to the lowest vibrational level of the first excited singlet state as well as to excited state reactions, solvent effects, energy transfer, and complex formations. Moreover, relaxation from the lowest level of the first excited singlet state to higher vibrational levels of the ground state also cause Stokes' shift.

The second general characteristic of fluorescence emission is that the emission spectrum is independent of the excitation wavelength because emission always occurs from the first

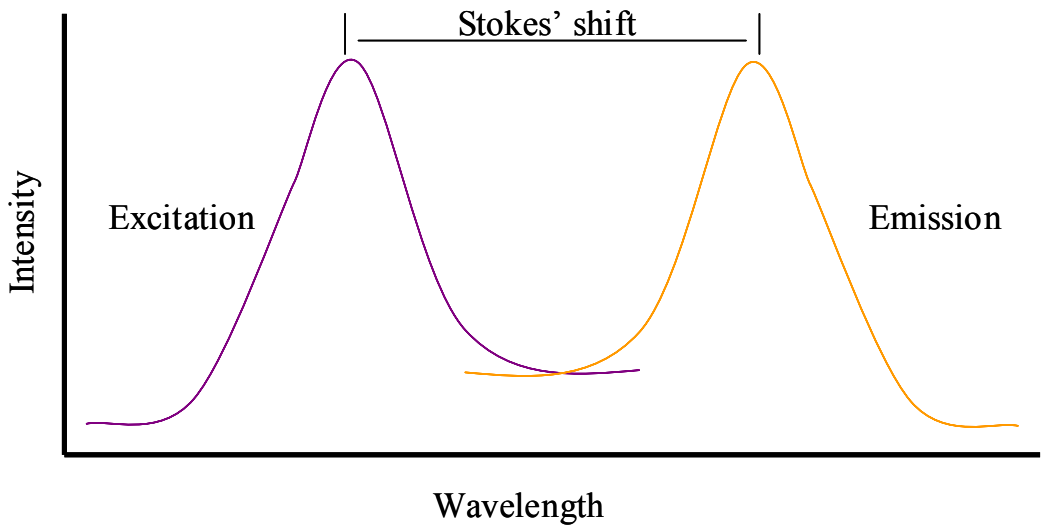

Figure 1.6 An example illustrating Stokes' shift.

excited singlet state. According to the Franck-Condon principle, the position of the nuclei does not change during any electronic transitions. Thus, the transition probability (Franck-Condon factor) of absorption between vibrational levels in the ground state and first excited singlet state is the exact same but reciprocal as that of emission [48]. In other words, the vibrational structure in excitation and emission bands is the same because there is no nuclear rearrangement. Therefore, the excitation and emission spectra obey the mirror image rule since electronic excitation does not significantly alter the spacing of vibrational levels. Typically, polycyclic aromatic hydrocarbons follow the mirror image rule. However, deviations are usually a result of nuclear rearrangements in the excited state or excited state reactions. For instance, if a molecule becomes more rigid while in the excited state then the emission spectrum will display more defined vibrational bands than the excitation spectrum, and thus the spectra will not be mirror images or indicative of reciprocal transitions.

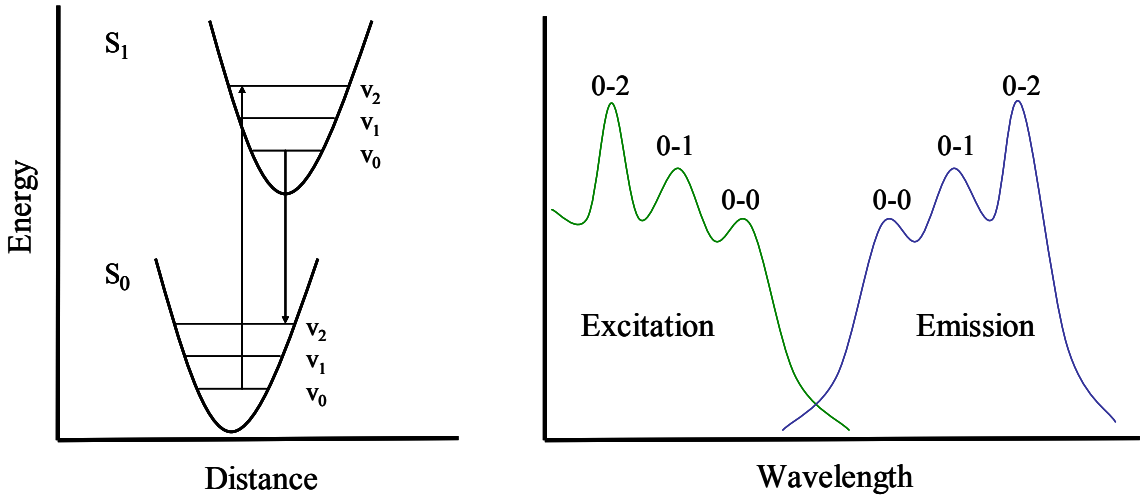

Figure 1.7 Mirror image rule and Franck-Condon principle.

1.2.3 Kinetics

Two important parameters—lifetime and quantum yield—are used to measure the kinetics of fluorescence. Fluorescence lifetime (τ) is the probability of finding a molecule in the excited state at a given time. In other words, it is the average time that a molecule will spend in the excited state. Fluorescence emission is a random process and few molecules will emit light at a time equal to the lifetime. The quantum yield (Φ_f) is the ratio of the number of photons emitted to the number of photons absorbed. In other words, it indicates what fraction of the total molecules absorbed will return to the ground state as fluorescence emission. It gives the efficiency of the fluorescence process.

Several deactivation processes such as intersystem crossing are constantly competing with fluorescence. Consequently, all molecules in the excited state will not return to the ground state by fluorescence emission. The intensity of absorbed light (I_a) is given by

$$I_a = I_o - I_t \tag{1.5}$$

where I_o is the intensity of the incident light and I_t is the intensity of transmitted light. If a sample is excited for a time longer than radiative and nonradiative deactivation processes, then the number of molecules in the first excited state will reach a steady state. So, the rate of absorption (Γ_a) will be equal to the rate of the deactivation processes, as shown by

$$\Gamma_a = \left(k_f + k_{vr} + k_{ic} + k_{isc} + k_q[Q]\right)[S_1] \tag{1.6}$$

where k_f, k_{vr}, k_{ic}, k_{isc}, and k_q are the rate constants for fluorescence, vibrational relaxation, internal conversion, intersystem crossing, and quenching, respectively. Furthermore, [Q] is concentration of the quencher while $[S_1]$ is the steady state concentration of molecules in the first excited singlet state.

The rate of fluorescence (Γ_f) is proportional to the rate of absorption by the following equation

$$\Gamma_f = \Phi_f \Gamma_a \tag{1.7}$$

since the quantum yield is the ratio of emitted photons to absorbed photons. Thus,

$$\Gamma_f = k_f[S_1] = \left[\left(k_f + k_{vr} + k_{ic} + k_{isc} + k_q[Q]\right)[S_1]\right]\Phi_f \tag{1.8}$$

Rearranging Equation 1.8 gives

$$\Phi_f = \frac{k_f}{k_f + k_{vr} + k_{ic} + k_{isc} + k_q[Q]} \tag{1.9}$$

If the rates for the nonradiative processes are much smaller than that of fluorescence, then the quantum yield approaches unity and most molecules will fluoresce. Generally, most molecules have quantum yields which are significantly less than unity.

Furthermore, the radiative or observed lifetime of the first excited singlet state is given as

$$\tau = \frac{1}{k_f + k_{vr} + k_{ic} + k_{isc} + k_q[Q]} \tag{1.10}$$

In the absence of nonradiative processes, the lifetime (τ_0) is given by

$$\tau_0 = \frac{1}{k_f} \tag{1.11}$$

By combining Equations 1.9 through 1.11, a relationship between the quantum yield and lifetime is derived, as shown by

$$\Phi_f = \frac{\tau}{\tau_0} \tag{1.12}$$

1.2.4 Linearity

Fluorescence intensity (I_f) is directly proportional to the intensity of light absorbed, as shown by

$$I_f = \Phi_f I_a = \Phi_f \left(I_o - I_t\right) \tag{1.13}$$

By combining Equations 1.1 and 1.2, Beer-Lambert's law can be expressed by

$$\frac{I_t}{I_o} = e^{-2.3\varepsilon bc} \tag{1.14}$$

Substitution of Equation 1.14 into 1.13 gives the fluorescence intensity as shown by

$$I_f = \Phi_f I_o \left(1 - e^{-2.3\varepsilon bc}\right) \tag{1.15}$$

After a Taylor series expansion of exponential term, the fluorescence intensity is given as

$$I_f = 2.3\,\Phi_f I_o\, \varepsilon bc \left[1 - \frac{2.3\varepsilon bc}{2!} + \frac{(2.3\varepsilon bc)^2}{3!} - \frac{(2.3\varepsilon bc)^3}{4!} + \ldots\right] \tag{1.16}$$

If εbc is small, i.e. ≤ 0.01, then the equation is reduced to

$$I_f = 2.3\Phi_f I_o \varepsilon bc \tag{1.17}$$

The fluorescence intensity is proportional to the absorbance and to the intensity of the incident light. However, the actual equation of fluorescence intensity includes instrumental parameters, as shown by

$$I_f = 2.3\Phi_f I_o \varepsilon bc f(\theta) g(\gamma) \tag{1.18}$$

where $f(\theta)$ is the instrumental collection efficiency and $g(\gamma)$ is the response factor for the detector and/or monochromators. Equation 1.18 is only valid at relatively low sample concentrations.

1.2.5 Influencing Factors

There are several factors which influence fluorescence intensity. Quantum yield, intensity of the incident light, absorption, and instrumental parameters have already been mentioned. However, there are other variables which have an effect on the efficiency of fluorescence such as pH, temperature, solvent, and molecular structure. These variables indicate that changes in the quantum yield are dependent on the fluorophore and its environment. For pH dependent fluorophores, ionization equilibrium will have an effect on the quantum yield because the electron distribution of the excited state will differ from that of the same fluorophore in its ground state. As a result, changes in the fluorescence intensity, wavelength maximum, and peak shape will be exhibited by the different ionization forms of the fluorophore. Moreoever, temperature has an effect on the quantum yield. Generally, increases in temperature will decrease the efficiency of the fluorescence process as a result of increases in collisional quenching. Likewise, decreases in temperature will increase the efficiency and decrease collisional quenching. Collisional quenching will be discussed in a later section.

The fluorescence of a fluorophore is also dependent on the solvent used. For example, decreases in solvent viscosity will decrease quantum yield as a result of increases in collisional quenching while increases in solvent viscosity will have the opposite effect. In addition, the electrostatic interactions, i.e. hydrogen bonding and dipole interactions, between the fluorophore

and solvent will have an effect on the quantum yield because of solvent reorientation effects. While in the excited state, the fluorophore's electron distribution is different than that of the ground state. So, the solvent molecules around the fluorophore must reorient themselves, which creates a metastable excited state and lowers the energy of the excited state. A metastable ground state is created during fluorescence. Then, the solvent molecules must reorient themselves again before the flourophore is able to return to its initial ground state. Stokes' shift is a result of solvent effects such as polarity and hydrogen bonding.

Molecular structure has an effect on quantum yield. Fluorescence is typically exhibited by molecules in which absorption results from $n \rightarrow \pi^*$ or $\pi \rightarrow \pi^*$ energy transitions. Other energy transitions are much less favorable for fluorescence. Aromatic and fused-ring compounds are some common fluorophores, and they usually fluoresce because of their conjugation and resonance stability. However, compounds containing halogens exhibit decreases in fluorescence as a result of increases in the occurrence of intersystem crossing. Moreover, the structural rigidity of a fluorophore has an effect on fluorescence. Because they have decreased interaction with solvent molecules, compounds which are more rigid have higher quantum yields than less rigid compounds.

As previously mentioned, quenching has a negative effect on fluorescence. Quenching is generally defined as any nonradiatve process which decreases fluorescence intensity. There are two types of quenching—dynamic and static. Dynamic or collisional quenching results when a molecule collides with other molecules or even with solvent molecules while in the excited state. As a result, the lifetime and fluorescence intensity of the fluorophore will decrease. The Stern-Volmer equation relates the effects of a quencher on fluorescence intensity, as show by

$$\frac{F_o}{F} = K_{sv}[Q] + 1 \tag{1.19}$$

where F_o is the fluorescence intensity in the absence of a quencher, F_o is the fluorescence intensity in the presence of a quencher, K_{sv} is the Stern-Volmer quenching constant, and [Q] is the quencher concentration. On the other hand, static quenching occurs when a ground state complex forms between the fluorophore and a quencher. Consequently, the fluorescence intensity of the fluorophore will decrease. However, the fluorescence lifetime of the fluorophore will remain the same because the quantum yield is unchanged due to the ground state complex formation. The Stern-Volmer equation for static quenching is

$$\frac{F_o}{F} = K_{eq}[Q] + 1 \tag{1.20}$$

where K_{eq} is the equilibrium constant for the ground state complex formation. Increases in temperature will decrease static quenching because the stability of the complex will decrease. Increases in temperature will increase molecular collisions and dynamic quenching.

1.2.6 Instrumentation

Figure 1.6 shows a schematic diagram of a typical fluorometer. The major instrumental components are the light source, excitation monochromator, sample holder, emission monochromator, detector, and computer. Xenon arc lamps, mercury lamps, and lasers are some typical light sources, but xenon arc lamps are more commonly used for general applications. Monochromators are generally used as the excitation and emission wavelength selectors due to their versatility. Even though photodiode arrays and charge-coupled devices can be used, most fluorometers employ photomultiplier tubes as detectors because they offer lower limits of detection. For a typical measurement, light from the lamp passes through the excitation monochromator, which transmits light that will excite the fluorophore. The fluorophore emits in all directions, however, fluorescence is only collected at a right angle. The emission monochromator is configured at a right angle to the excitation light in order to reduce

interferences from the light source and scattering from the sample solution. After passing through the emission monochromator, the emitted light is collected by a detector and the spectral data is recorded on a computer.

1.3 Chemometrics

Following a plethora of data acquired in analytical chemistry due to the use of more advanced computers, the science of chemometrics was formed. In 1972, Svante Wold and Bruce R. Kowalski coined the term *chemometrics* [50]. According to the International Chemometrics Society, chemometrics is the application of mathematical and statistical techniques for chemical data analysis [51, 52]. It designs or selects optimal procedures and experiments as well as provides maximum chemical information of chemical data.

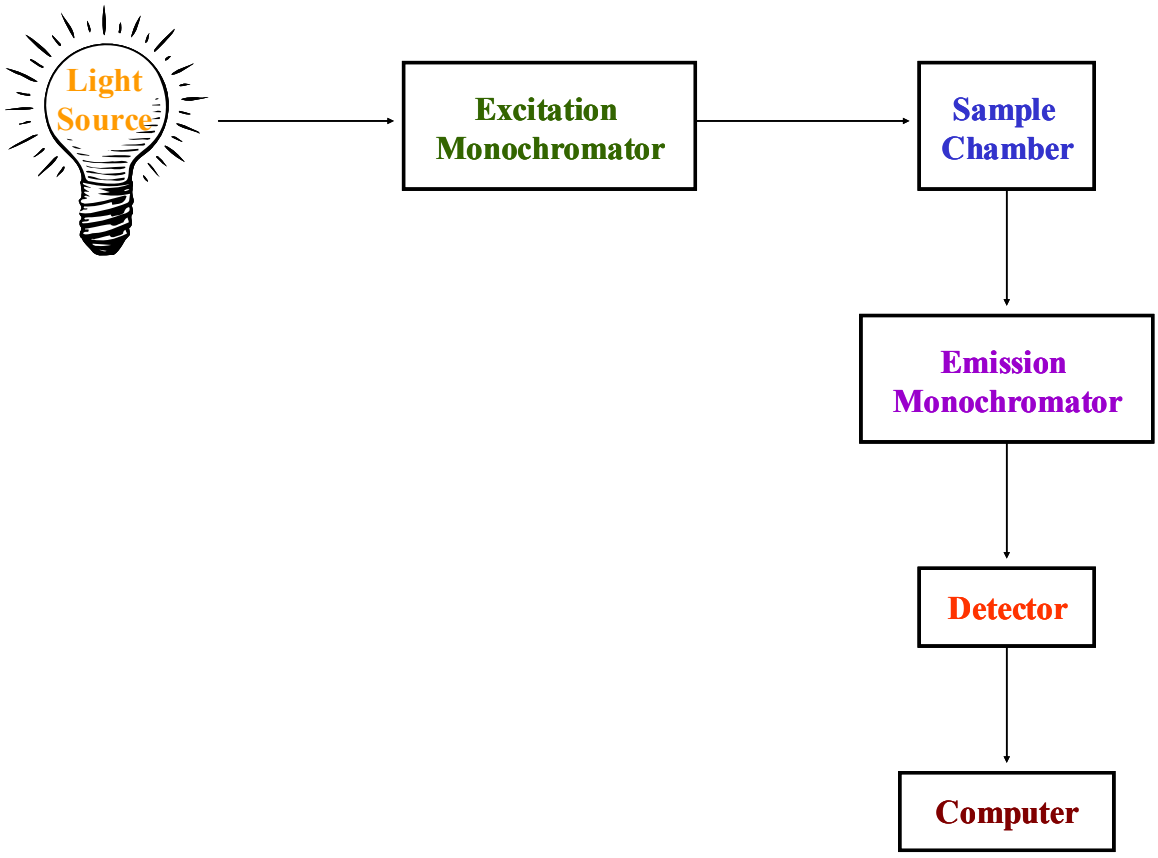

Figure 1.8 Schematic diagram of a typical fluorimeter.

In other words, chemometrics can be used for studying trends in chemical data and for developing calibrations for chemical data. Pattern recognition and regression calibration are two major classes of chemometrics. Pattern recognition involves grouping or classifying data according to similar patterns or function. For instance, the periodic table of contents is an example of pattern recognition since the elements are grouped according to similar characteristics. On the other hand, regression calibration involves developing a regression model which accurately describes and predicts the data. In other words, it finds a suitable mathematical relationship between independent and dependent variables.

1.3.1 Multivariate Regression Modeling

Univariate linear regression and multivariate linear regression modeling are two main types of regression modeling. For univariate linear regression modeling, the association between one dependent variable (y) and one independent variable (x) is given by

$$y = b_o + b_1 x \tag{1.21}$$

where b_o and b_1 are the intercept and slope, respectively. However, if more than one independent variable is present, then multivariate linear regression modeling is needed. Multivariate regression methods such as principal component regression (PCR) and partial-least-squares regression (PLS-1), are commonly used for several applications in analytical chemistry. In general, multivariate regression modeling relates one dependent variable y with more than one independent variables x by a linear relationship, as show by

$$y = b_o + b_1 x_1 + b_2 x_2 + \ldots + b_n x_n \tag{1.22}$$

where b_n is the regression model coefficient. Equation 1.22 can be expressed in shorthand matrix notation as

$$Y = XB \tag{1.23}$$

where Y is the matrix of dependent variables, X is the matrix of independent variables, and B is the matrix of regression coefficients. Multivariate regression modeling can be used to predict future values of Y after the regression coefficient B is determined.

However, a problem with multivariate regression modeling is colinearity or correlation among the independent x variables. To avoid this problem, all multivariate regression methods require an orthogonal basis set or coordinate system on which the data can be represented. PCR and PLS-1 techniques use projection methods to acquire a series of variance-scaled eigenvectors which represent the data as a new coordinate system. During data decomposition, the dimensionality of the data is reduced because only the major components (eigenvectors) are used to represent the data. For the PLS-1 technique, data decomposition includes the dependent variable y. In fact, PLS-1 is commonly used for correlating changes in spectral data with changes in known composition. This regression technique reduces sample response prediction error by extracting successive linear combinations of the predictors. Therefore, PLS-1 is able to account for factors which explain variations in the responses and the predictors.

Multivariate regression modeling is a two-step process. For step one, or the calibration phase, a calibration regression model is developed with a calibration set of samples with known compositions. In this thesis, fluorescence spectra of calibration samples with known amino acid enantiomeric composition are collected over a certain wavelength range. Changes in spectral data from the calibration set are correlated with the known enantiomeric compositions. For step two, or the validation phase, the calibration regression model developed in the first step is tested with an independently prepared validation set of samples with known enantiomeric compositions. The validation set of samples has different enantiomeric compositions than that of the calibration set, and the spectra of the validation set are collected over the same wavelength

range as the calibration set. In the validation phase, spectral data from validation set are used to predict the enantiomeric compositions of the validation samples.

1.4 Scope of Thesis

A chiral pinanediol-derived boronate resorcinarene macrocycle was developed by Lewis et. al. [53]. The use of boronic acid based resorcinarene macrocycles for achiral and chiral carbohydrate recognition and chemical sensing using UV-visible spectroscopy has been previously reported [54-57]. Consequently, these macrocycles could be useful in investigating the fluorescence detection and enantiodiscrimination of amino acids. While a majority of fluorescent chiral recognition involving amino acids has been performed with amino acid derivatives [58-60], the chiral recognition ability of a fluorescent resorcinarene macrocycle with unmodified amino acids was studied in this thesis. Amino acids, which are structurally identical to one another, but have different side chains, are among the most important molecules in biological systems because they are also constituents of peptides, proteins, and DNA. Most amino acids exhibit transparency in the UV-visible region. Therefore, fluorescence enantioselective recognition studies of unmodified amino acids would be an attractive approach for monitoring diseases and protein biological functions. In addition, many approaches have recently demonstrated that the enantiomeric composition of chiral molecules can be determined by multivariate regression modeling of fluorescence emission spectral data [61-64]. These results from spectral data measurements have demonstrated that multivariate regression modeling is a reliable method for evaluating the chiral recognition ability of chiral molecules.

This thesis reports the fluorescent spectral properties of a tetraarylboronate resorcinarene macrocycle (TBRM) and investigates the enantiomeric selectivity of unmodified amino acids with TBRM employed as a chiral selector. In addition, the chiral recognition ability of TBRM

with selected amino acids as well as determination of enantiomeric composition of lysine was evaluated by use of steady-state fluorescence spectroscopy and multivariate regression analysis.

CHAPTER 2

EXPERIMENTAL

2.1 Materials

D- and L-enantiomers of alanine, arginine, asparagine, aspartate, glutamine, glutamate, isoleucine, leucine, lysine, methionine, proline, serine, threonine, and valine were obtained from Sigma-Aldrich (St. Louis, MO) and used as received. Spectroscopic grade acetonitrile, dimethyl sulfoxide, ethyl acetate, methanol, and tetrahydrofuran were also purchased from Sigma Aldrich (St. Louis, MO). Resorcinol, 4-formylphenylbornonic acid, ethanol, hydrochloric acid, dimethyl formamide, sodium sulfate, and 1R, 2R, 3S, 5R-(-)-pinanediol were obtained from Sigma Chemical Company (Milwaukee, WI). The purity of all analytes and reagents was 99% or higher.

2.2 Synthesis

The chiral (-)-pinanediol tetraarylboronate resorcinarene macrocycle was synthesized according to the procedure described by Lewis et. al. [53] and shown in Scheme 1. The macrocycle was synthesized from resorcinol (**1**) and 4-formylphenylboronic acid (**2**) in a water/ethanol/concentrated HCl mixture. This solution was stirred at 75^{o}C for 24 hr under N_2, cooled in an ice bath for an hour, and then filtered. The resulting precipitate contained two isomers (**3, 4**) which were separated by fractional crystallization. Chirality was added to the desired isomer by mixing it with 1R, 2R, 3S, 5R-(-)-pinanediol (**5**), DMF, and Na_2SO_4 under N_2 at 85^{o}C for 48 hr. The mixture was cooled to room temperature and filtered. The filtrate was dried, slurried in ether, filtered, and dried again to obtain the final product (**6**). Product formation was confirmed using proton NMR.

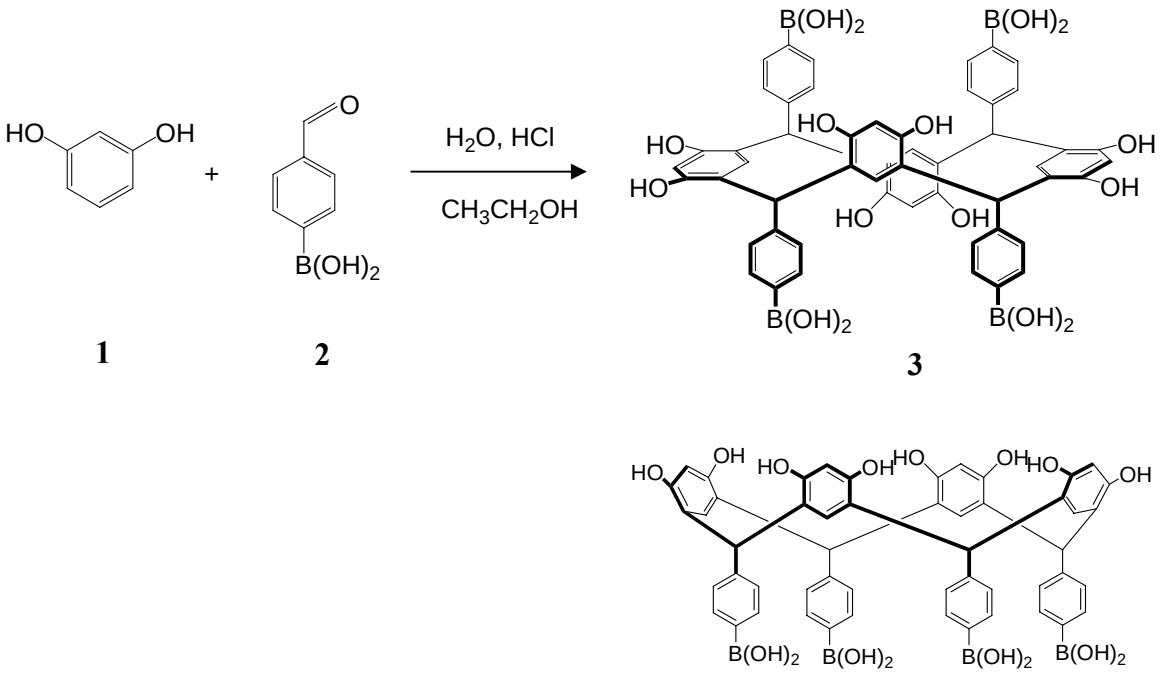

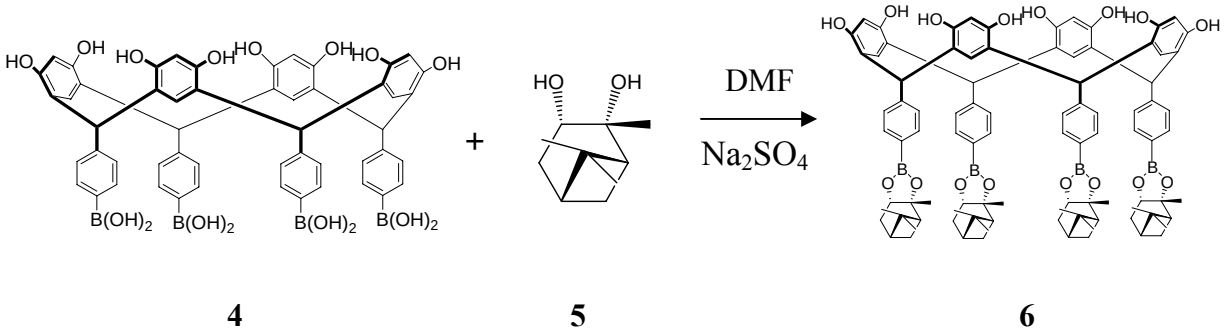

Scheme 2.1: Synthesis of chiral macrocycle TBRM.

2.3 Sample Preparation

Stock solutions of TBRM in spectroscopic grade methanol and each amino acid in carbonate buffer (pH 7.2) were prepared. For the polarity study, an individual standard solution of the chiral macrocycle (7 μM) was prepared in different solvents. In addition, a series of different standard solutions of TBRM were prepared in methanol for determining the fluorescence quantum yield of the chiral macrocycle. For the enantiomeric selectivity of amino acids, mixtures of chiral macrocycle (7 μM) and amino acid (1 mM) were also prepared in methanol (90 %) and water (10 %). All standard solutions were made in triplicate. For chemometrics experiments, the final concentration of all calibration and validation solutions contained fixed macrocycle (7 μM) and amino acid (2 mM) enantiomer concentrations. The enantiomeric composition of the calibration samples ranged from 0.05 to 0.95 mol fraction.

2.4 Data Analysis

Multivariate data analysis was achieved using the Unscrambler™ (vers 9.1; CAMO, Inc., Corvalis, OR). Partial-least square-regression models (PLS-1) were developed from the spectral data of guest-host complexes using full-cross validation. The models were validated with independently prepared test solutions containing known mole ratios of lysine.

2.5 Instrumentation

Steady-state fluorescence measurements were performed in triplicate at room temperature using a Spex Fluorolog-3 spectrofluorometer (model FL3-22TAU3, Jobin Yvon, Edison, NJ) equipped with a 450-W xenon lamp, double grating excitation and emission monochromators, and a R928P photomultiplier tube detector. Excitation and emission spectra were acquired using 10 mm quartz fluorometer cell with excitation bandpass set at 1 nm and emission bandpass at 4 nm. The excitation and emission wavelengths were monitored at 290 and 435 nm, respectively, for the chiral macrocycle. In addition, absorbance measurements were made in triplicate at room

temperature using a UV-3101 PC (UV-VIS NIR) scanning spectrophotometer (Shimadzu, Columbia, MD) equipped with a deuterium halogen lamp. The absorbance spectra were recorded in 10 mm quartz cell. Both fluorescence and absorption spectra were blank subtracted before proceeding with the data analysis.

CHAPTER 3

RESULTS AND DISCUSSION

3.1 Fluorescence Characteristics of Macrocycle

Fluorescence spectroscopic properties, including emission and excitation characteristics and quantum yield of TBRM, were investigated. The influence of different solvents on the chiral macrocycle's microenvironment was evaluated. Different solvents, including acetonitrile, dimethyl sulfoxide (DMSO), ethyl acetate, methanol, and tetrahydrofuran, were used in order to study the fluorescence characteristics of TBRM. Significant shifts in fluorescence spectra of the chiral macrocyle in the presence of each solvent were observed at the maximum emission wavelength. The TBRM maximum emission wavelengths in tetrahydrofuran, ethyl acetate, acetonitrile, DMSO, and methanol were 325, 350, 390, 410, and 435 nm, respectively. In general, these marked shifts in the maximum emission wavelength are indicative of non-covalent interactions between the solvent molecules and the chiral macrocycle.

The quantum yield of the TBRM was determined in order to evaluate its fluorescence efficiency. For determination of the TBRM fluorescence quantum yield, L-tryptophan (L-Trp) was selected as a standard sample since L-Trp absorbs near the excitation wavelength ($\lambda_{max\ ex}$ = 290 nm) of the chiral macrocycle. As a result, it is expected that the same number of photons will be absorbed by both samples. Dilute solutions of TBRM (1 μM - 10μM) and L-Trp (4 μM – 22 μM) were prepared in methanol and water, respectively. The fluorescence of the standard and unknown were recorded using the same standard and unknown solutions used for absorbance measurements.

The quantum yield of the chiral macrocycle was determined using Williams' comparative method and calculated from the following equation [65]

$$\Phi_x = \Phi_{std} \, (Grad_x / Grad_{std}) \, (\eta_x^2 / \eta_{std}^2) \qquad (1.24)$$

where *x* and *std* subscripts denote the chiral macrocycle (unknown) and L-Trp (used as the standard), respectively, Φ is the quantum yield, *Grad* is the slope from the plot of integrated fluorescence intensity versus absorbance (Appendix A), and η is the refractive index. The quantum yield of L-Trp has been previously reported in water as 0.14 [66]. The refractive indices for water and methanol are 1.32 and 1.33, respectively. Using equation 1, the calculated quantum yield of TBRM at a maximum emission wavelength of 435 nm was 0.10, indicative of a relatively highly fluorescence efficienct macrocycle. In addition, a molar absorptivity value of 16,800 M^{-1} cm^{-1} was obtained for TBRM, indicating that the chiral macrocycle is a strong absorber (Appendix B).

3.2 Amino Acid Chiral Recognition

The enantiomeric selectivity of the chiral macrocycle towards different amino acids was examined. Spectral differences of TBRM (7 μM) with the investigated amino acids (1 mM) were obtained as illustrated in Figure 3.1. Fluorescence intensity (ΔI) was acquired by subtracting the emission peak of TBRM from that of the TBRM and amino acid mixture at 435 nm. In general, it was observed that the fluorescence intensity of the macrocycle was higher in the presence of L-amino acid enantiomers as compared to D-amino acids. This is indicative of the higher enantiomeric selectivity of the TBRM towards L-amino acids in contrast to D-amino acids. However, an opposite trend was observed in the fluorescence intensity for TBRM with L-Arginine, L-Glutamate, and L-Proline. Interestingly, the difference in the fluorescence intensity of the macrocycle in the presence of D- and L-Lysine was the highest as compared to all investigated amino acids.

Various degrees of enantioselectivity for amino acids were observed as illustrated in Figure 3.1. The chiral recognition of amino acids is based on the formation of diastereomeric complexes between the enantiomer and the chiral macrocycle as indicated by differences in the

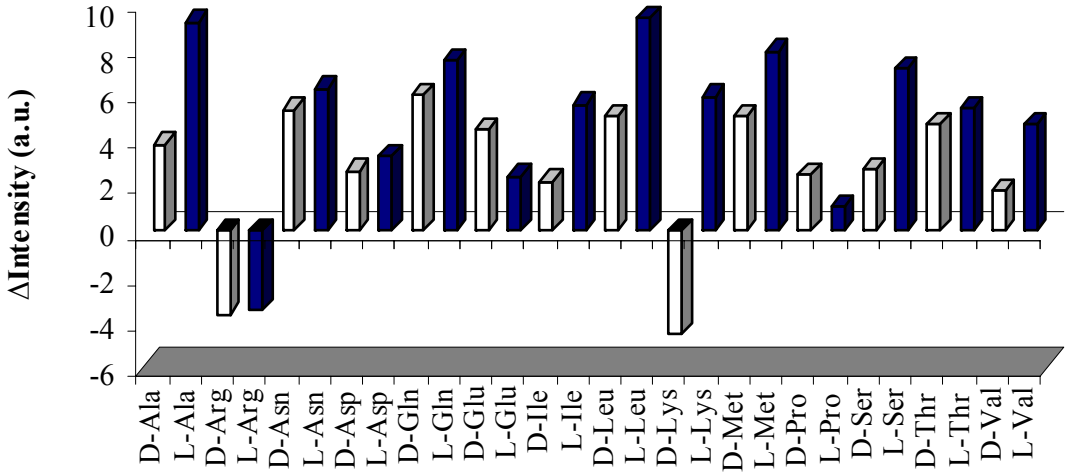

Figure 3.1 Enantiomeric selectivity of the chiral macrocycle towards different amino acids. λ_{em} = 435 nm

fluorescence emission of TBRM with amino acid enantiomers. It is observed that there were significant differences in fluorescence intensity of TBRM with alanine, leucine, and lysine enantiomers as compared to less evident changes for arginine, aspartate, and asparagine enantiomers. Moreover, all amino acids used in this study do not absorb in the same region as the chiral macrocycle, further supporting that the changes in fluorescence intensity were due to the interactions between the macrocycle and amino acid enantiomers.

As noted above, the enantiomeric selectivity of the macrocycle was the highest towards L-Lysine (L-Lys) as compared to all other amino acids investigated. This high chiral recognition ability of TBRM for lysine can be attributed to the excitation spectra of the macrocycle with lysine in which there is not only a peak at 290 nm but also a peak at 350 nm (Figure 3.2A), suggesting complex formation with TBRM and lysine. At 290 nm, the excitation intensity of TBRM is decreased in the presence of D-Lys while it is increased in the presence of L-Lys. However, at 350 nm the excitation intensity of TBRM with L-Lys is higher than that of TBRM with D-Lys. An excitation peak around 350 nm was not observed in the spectrum of TBRM with

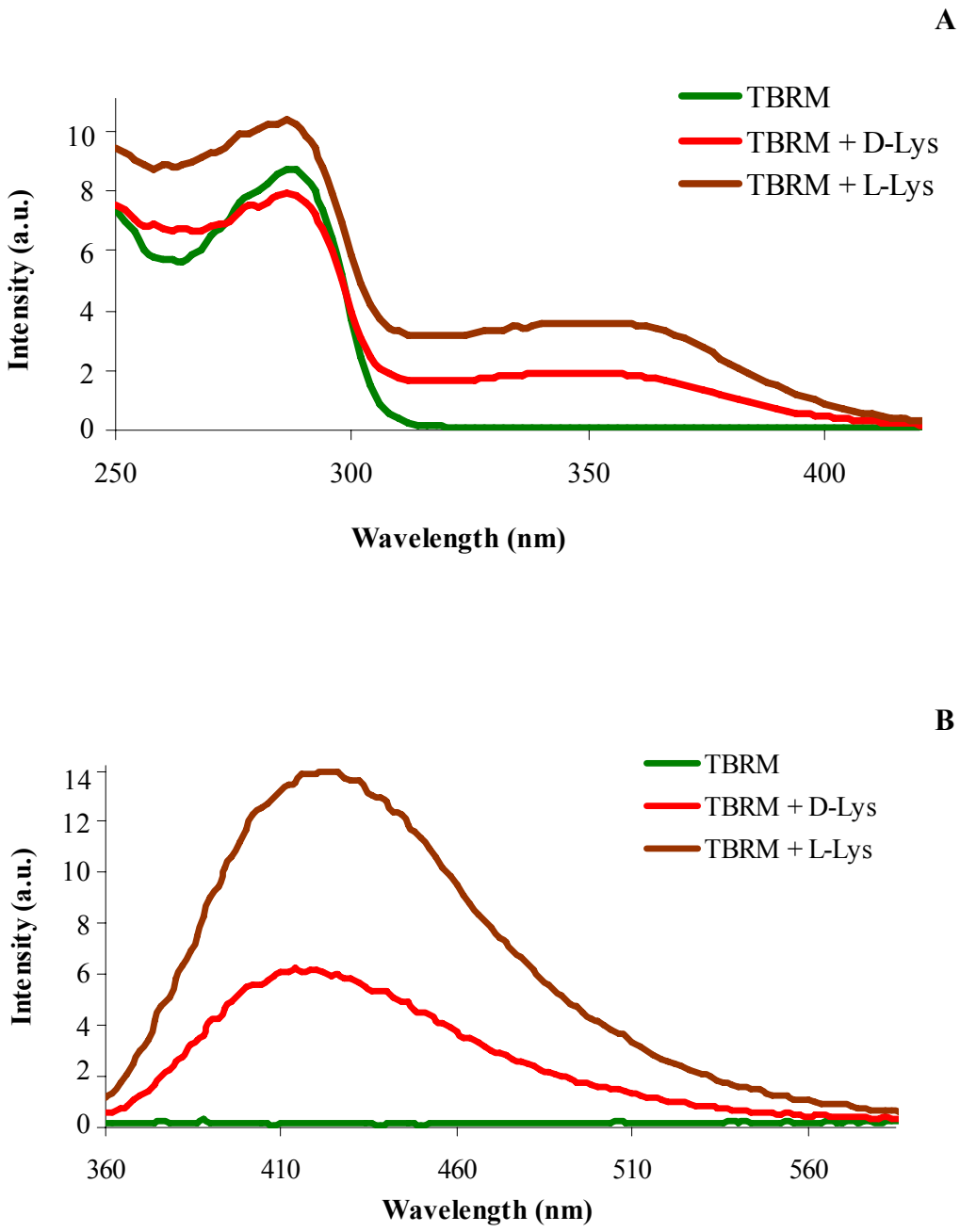

Figure 3.2 (A) Excitation spectra of macrocycle (7 μM) in the absence and presence of D-Lysine (1 mM) and L-Lysine (1 mM); λ_{em} = 435 nm; (B) Emission spectra of macrocycle in the absence and presence of D-Lys (1 mM) and L-Lys (1 mM); λ_{exc} = 350nm.

any other amino acids investigated. The peak at 350 nm was investigated by collecting the emission at an excitation of 350 nm (Figure 3.2B). As a result, no fluorescence emission was observed for the macrocycle in the absence of amino acid at this excitation wavelength. For the macrocycle and D-Lys (or L-Lys) mixture, however, an emission spectrum with a maximum fluorescence intensity at 420 nm was observed. In addition, the emission intensity of the macrocycle with L-Lys was higher than that with D-Lys.

3.3 Determination of Enantiomeric Composition

Accurate determination of the enantiomeric composition of amino acids is important, particularly for the pharmaceutical industry, because D-amino acids have been detected at low concentrations in humans, which may have an antagonistic biological function. In addition, deficiencies in L-lysine concentrations have been reported to result in mental retardation and hyperammonemia [67, 68]. However, an increase in L-lysine concentrations can prevent the recurrence of herpes simplex infections [69].

In this phase of the study, fluorescence steady-state based measurements were used to determine the enantiomeric composition of chiral molecules. As previously noted, the enantiomeric selectivity of the chiral macrocycle was highest with lysine as compared to other amino acids. To further understand the chiral recognition ability of the chiral macrocycle towards lysine, determination of the enantiomeric composition was investigated for lysine using partial-least-squares regression modeling (PLS-1). Multivariate regression modeling allows quick and accurate screenings of chiral molecules, and it has been widely used for correlating spectral variations with known compositional changes. According to procedures from previous studies [61-63, 70], PLS-1 regression modeling was used to correlate changes in spectral data of guest-host complexes with enantiomeric composition of samples.

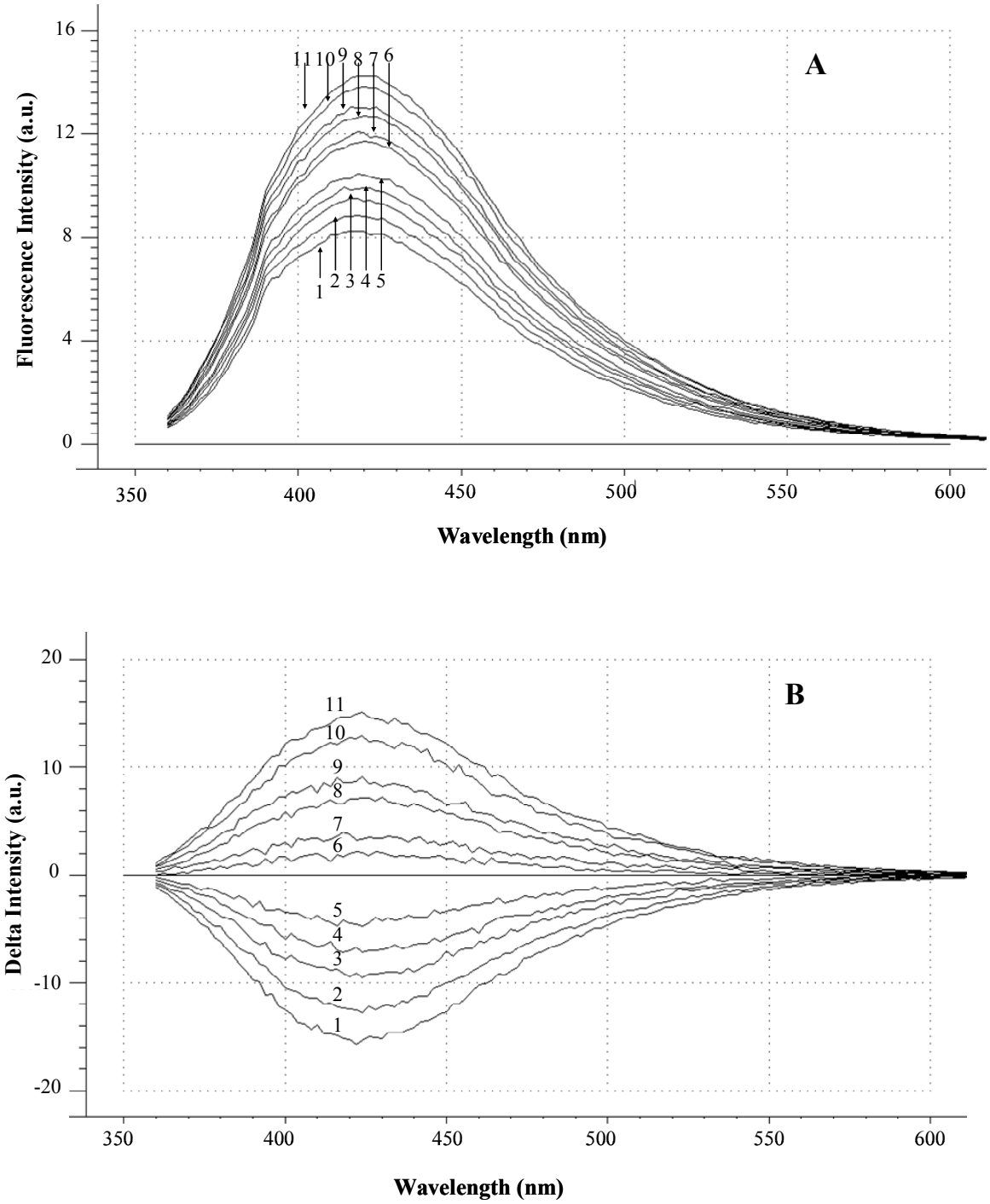

Figure 3.3 (A) Fluorescence spectra of 11 solutions of lysine and the macrocycle with a total lysine concentration of 2 mM but different enantiomeric compositions; λ_{exc} = 350nm. Mol fraction of L-lysine: (1) 0.0; (2) 0.1; (3) 0.2; (4) 0.3; (5) 0.4; (6) 0.5; (7) 0.6; (8) 0.7; (9) 0.8; (10) 0.9; (11) 1.0.; (B) Mean-centered plots of 11 solutions containing the macrocycle and lysine in Figure 3.3A.

Figure 3.3A illustrates the emission spectra of different mixtures containing a fixed concentration of the macrocycle (7μM) and lysine (2 mM) with varying the enantiomeric composition of lysine. The samples have a maximum emission at 420 nm. Spectral variations of the macrocycle were observed with different enantiomeric compositions of lysine. Again, this finding is indicative of the formation of diastereomers in the different samples. In addition, this is further confirmed by a mean-centered plot (Figure 3.3B) obtained by averaging the spectral data of the mixtures (Figure 3.3A) and subsequently subtracting the average spectrum from each individual sample spectrum on a wavelength by wavelength basis [63]. Mean-centered plots offer better insight into the spectral variations of TBRM which occurred with different enantiomeric compositions of lysine. It is also interesting to note that the spectral data of samples with enantiomeric compositions of L-Lys greater than 0.5 mol fractions are above the plot's origin while those with mol fractions less than 0.5 are below the origin, as illustrated in Figure 3.3B.

The above findings are also supported by multivariate regression modeling. From PLS-1, the correlation coefficient (0.9932), the slope (1.0158), and the offset (0.0168) were obtained from the calibration regression modeling. A perfect model would have a correlation coefficient of 1, a slope of 1, and an offset of 0. The results of the actual mole ratio, predicted mole ratio, and percent relative error obtained from the independent test solutions of D-Lysine and L-Lysine in the validation study are summarized in Table 1. Root-mean-square percent relative error (*RMS%RE*) was used to evaluate the overall prediction ability of the calibration model for the enantiomeric composition determination of lysine. The root-mean-square percent relative error is given by the following equation

$$RMS\%RE = \sqrt{\frac{\sum (\%RE_i)^2}{n}} \tag{1.25}$$

where $\%RE_i$ is the percent relative error determined from the known and predicted values for the *i*th sample in the validation set, and *n* is the number of validation samples in the set. From Table 1, it is observed that the prediction of D-Lysine (*RMS%RE*, 5.8%) was better than that for L-Lysine (*RMS%RE*, 12%).

Table 1 Actual and predicted mol fraction of D-Lysine and L-Lysine for solutions containing 2 mM lysine and 7 μM macrocycle

D-Lysine			L-Lysine		
Actual mol fraction	Predicted mol fraction	Relative error (%)	Actual mol fraction	Predicted mol fraction	Relative error (%)
0.050	0.049	1.76	0.950	0.951	-0.110
0.150	0.157	-4.67	0.850	0.843	0.820
0.250	0.230	8.00	0.750	0.770	-2.67
0.350	0.308	12.0	0.650	0.692	-6.46
0.450	0.448	0.410	0.550	0.552	-0.360
0.550	0.540	1.82	0.450	0.460	-2.22
0.650	0.589	9.38	0.350	0.411	-17.4
0.750	0.773	-3.07	0.250	0.227	9.20
0.850	0.851	-0.120	0.150	0.149	0.670
0.950	0.996	-1.68	0.050	0.034	31.6
RMS%RE		5.80	RMS%RE		12.0

CHAPTER 4

CONCLUSIONS AND FUTURE STUDIES

4.1 Conclusions

The results from the present study demonstrated a successful investigation of a chiral resorcinarene macrocycle and its selective chiral interactions with amino acid enantiomers. The chiral macrocycle had a quantum yield of 0.10 indicating relatively good fluorescence efficiency. In addition, the chiral recognition ability of the macrocycle was examined with 14 pairs of amino acid enantiomers. Examination of the results suggests that the enantiomeric selectivity of the chiral macrocycle towards lysine was highest as compared to other amino acids. This finding was accurately predicted using host-guest chemistry, fluorescence spectroscopy, and multivariate regression modeling. Moreover, the macrocycle has potential applications for rapid screening of amino acids and can be used as an off and on sensor for D- and L-Lysine.

4.2 Future Studies

Future directions should be focused on understanding the mechanism of chiral recognition of the macrocycle towards the investigated amino acids, particularly lysine. Moreover, several analytical methods such as capillary electrophoresis, time-resolved fluorescence lifetime, and fluorescence anisotropy, can be applied in order to examine the mechanism of the chiral macrocycle with amino acids. These methods may provide a different and better understanding about the enantiomeric discrimination of chiral macrocycle towards the amino acids. In addition, the use of the macrocycle as a fluorescent chiral selector for other classes of molecules such as chiral drugs should be investigated in the future. As was previously discussed, the macrocycle can be used as a sensor for lysine. Another interesting pursuit would be a steady-state fluorescence investigation of the macrocyle as an indicator for exposed lysine residues on proteins such as cytochrome c and human serum albumin.

REFERENCES

[1] T. W. G. Solomons (1996) Organic Chemistry, John Wiley & Sons, New York.

[2] L. Pasteur, *Ann. Chim. Phys.* **24,** 442 (1848).

[3] B. Buszewski, M. Jezierska-Switala, and S. Kowalska, *Journal of Chromatography B-Analytical Technologies in the Biomedical and Life Sciences* **792,** 279 (2003).

[4] K. Imai, *Yakugaku Zasshi-Journal of the Pharmaceutical Society of Japan* **123,** 901 (2003).

[5] H. Onouchi, T. Hasegawa, D. Kashiwagi, H. Ishiguro, K. Maeda, and E. Yashima, *Journal of Polymer Science Part a-Polymer Chemistry* **44,** 5039 (2006).

[6] C. Pena, I. Alfonso, B. Tooth, N. H. Voelcker, and V. Gotor, *Journal of Organic Chemistry* **72,** 1924 (2007).

[7] M. Ravikumar, S. Prabhakar, and M. Vairamani, *Chemical Communications***,** 392 (2007).

[8] J. J. Sheng, A. Saxena, and M. W. Duffel, *Drug Metabolism and Disposition* **32,** 559 (2004).

[9] I. Kaneko, N. Yamada, Y. Sakuraba, M. Kamenosono, and S. Tutumi, *Journal of Neurochemistry* **65,** 2585 (1995).

[10] J. T. Powell, N. Vine, and M. Crossman, *Atherosclerosis* **97,** 201 (1992).

[11] R. Shapira, and C. H. J. Chou, *Biochemical and Biophysical Research Communications* **146,** 1342 (1987).

[12] J. Jacques (1993) The Molecule and Its Double, McGraw-Hill, Inc., New York.

[13] F. Jamali, R. Mehvar, and F. M. Pasutto, *Journal of Pharmaceutical Sciences* **78,** 695 (1989).

[14] R. Crossley (1995) Chirality and the Biological Activity of Drugs, CRC Press, New York.

[15] W. Lenz, *Teratology* **38,** 203 (1988).

[16] U. S. F. D. A, *Chirality* **4,** 338 (1992).

[17] M. C. K. V. Ramos, E. F. Silva, F. R. Aquino Neto, E. P. Pecanha, C. R. Rodrigues, E. J. Barreiro, and C. A. M. Fraga, *Anal. Chem.* **72,** 3056 (2000).

[18] M. D. Ramos, L. H. P. Teixeira, F. R. D. Neto, E. J. Barreiro, C. R. Rodriguez, and C. A. M. Fraga, *Journal of Chromatography A* **985,** 321 (2003).

[19] I. Slama, C. Dufresne, E. Jourdan, F. Fahrat, A. Villet, A. Ravel, C. Grosset, and E. Peyrin, *Anal. Chem.* **74,** 5205 (2002).

[20] C. Yamamoto, S. Inagaki, and Y. Okamoto, *Journal of Separation Science* **29,** 915 (2006).

[21] H. Matsunaga, Y. Sadakane, and J. Haginaka, *Electrophoresis* **24,** 2442 (2003).

[22] M. C. Vescina, A. M. Fermier, and Y. Guo, *Journal of Chromatography A* **973,** 187 (2002).

[23] W. H. Pirkle, P. G. Murray, D. J. Rausch, and S. T. McKenna, *J. Org. Chem.* **61,** 4769 (1996).

[24] E. Yashima, C. Yamamoto, and Y. Okamoto, *J. Am. Chem. Soc.* **118,** 4036 (1996).

[25] M. Sawada, Y. Takai, H. Yamada, J. Nishida, T. Kaneda, R. Arakawa, M. Okamoto, K. Hirose, T. Tanaka, and K. Naemura, *Journal of the Chemical Society-Perkin Transactions 2***,** 701 (1998).

[26] K. A. Schug, N. M. Maier, and W. Lindner, *Chemical Communications***,** 414 (2006).

[27] C. Z. Wang, Z. A. Zhu, Y. Li, Y. T. Chen, X. Wen, F. M. Miao, W. L. Chan, and A. S. C. Chan, *New Journal of Chemistry* **25,** 801 (2001).

[28] K. Luo, H. Y. Jiang, J. S. You, Q. X. Xiang, S. J. Guo, J. B. Lan, and R. G. Xie, *Letters in Organic Chemistry* **3,** 363 (2006).

[29] O. Rusin, O. Alpturk, M. He, J. O. Escobedo, S. Jiang, F. Dawan, K. Lian, M. E. McCarroll, I. M. Warner, and R. M. Strongin, *Journal of Fluorescence* **14,** 611 (2004).

[30] O. Rusin, V. Kral, J. O. Escobedo, and R. M. Strongin, *Organic Letters* **6,** 1373 (2004).

[31] K. Hamasaki, S. Usui, H. Ikeda, T. Ikeda, and A. Ueno, *Supramolecular Chemistry* **8,** 125 (1997).

[32] M. Karakaplan, and T. Aral, *Tetrahedron: Asymmetry* **16,** 2119 (2005).

[33] M. S. Pena, Y. L. Zhang, and I. M. Warner, *Analytical Chemistry* **69,** 3239 (1997).

[34] L. Pu, *Chem. Rev.* **104,** 1687 (2004).

[35] P. Timmerman, W. Verboom, and D. N. Reinhoudt, *Tetrahedron* **52,** 2663 (1996).

[36] A. Baeyer, *Ber. Dtsch. Chem. Ges.* **5,** 25 (1872).

[37] A. Baeyer, *Ber. Dtsch. Chem. Ges.* **5,** 280 (1872).

[38] J. B. Niederl, and H. J. Vogel, *J. Am. Chem. Soc.* **62,** 2512 (1940).

[39] H. Erdtman, and S. Hogberg, *Tetrahedron Letters***,** 1679 (1968).

[40] Y. Aoyama, *Trac-Trends in Analytical Chemistry* **12,** 23 (1993).

[41] Y. Aoyama, Y. Tanaka, H. Toi, and H. Ogoshi, *Journal of the American Chemical Society* **110,** 634 (1988).

[42] A. Jasat, and J. C. Sherman, *Chemical Reviews* **99,** 931 (1999).

[43] K. Kobayashi, M. Tominaga, Y. Asakawa, and Y. Aoyama, *Tetrahedron Letters* **34,** 5121 (1993).

[44] H. J. Schneider, and U. Schneider, *Journal of Inclusion Phenomena and Molecular Recognition in Chemistry* **19,** 67 (1994).

[45] W. H. Pirkle, and T. C. Pochapsky, *Chem. Rev.* **89,** 347 (1989).

[46] L. Salem, X. Chapuisat, G. Segal, P. C. Hiberty, C. Minot, C. Leforestier, and P. Sautet, *J. Am. Chem. Soc.* **109,** 2887 (1987).

[47] E. H. Easson, and E. Stedman, *J. Biochem.* **27,** 1257 (1933).

[48] J. R. Lakowicz (1999) Principles of Fluorescence Spectroscopy 2nd ed., Kluwer Academic/Plenum, New York.

[49] G. G. Guilbault (1990) Practical Fluorescence, 2nd ed., Marcel Dekker, Inc., New York.

[50] D. L. Massart, B. G. M. Vandeginste, S. N. Deming, Y. Michotte, and L. Kaufman (1988) Chemometrics: a textbook, Amsterdam.

[51] M. Otto (1999) Chemometrics: Statistics and Computer Application in Analytical Chemistry, Wiley-VCH, New York.

[52] K. R. Beebe, R. J. Pell, and M. B. Seasholtz (1998) Chemometrics: A Practical Guide, John Wiley & Sons, Inc., New York.

[53] P. T. Lewis, C. J. Davis, M. C. Saraiva, W. D. Treleaven, T. D. McCarley, and R. M. Strongin, *J. Org. Chem.* **62,** 6110 (1997).

[54] C. J. Davis, P. T. Lewis, M. E. McCarroll, M. W. Read, R. Cueto, and R. M. Strongin, *Org. Lett.* **1,** 331 (1999).

[55] M. He, R. J. Johnson, J. O. Escobedo, P. A. Beck, K. K. Kim, N. N. St. Luce, C. J. Davis, P. T. Lewis, F. R. Fronczek, B. J. Melancon, A. A. Mrse, W. D. Treleaven, and R. M. Strongin, *J. Am. Chem. Soc.* **124,** 5000 (2002).

[56] P. T. Lewis, C. J. Davis, L. A. Cabell, M. He, M. W. Read, M. E. McCarroll, and R. M. Strongin, *Org. Lett.* **2,** 589 (2000).

[57] T. Z. Zhang, and E. V. Anslyn, *Organic Letters* **8,** 1649 (2006).

[58] J. Lin, Z.-B. Li, H.-C. Zhang, and L. Pu, *Tetrahedron Letters* **45,** 103 (2004).

[59] J. Lin, A. R. Rajaram, and L. Pu, *Tetrahedron* **60,** 11277 (2004).

[60] W. L. Wong, K. H. Huang, P. F. Teng, C. S. Lee, and H. L. Kwong, *Chemical Communications***,** 384 (2004).

[61] S. O. Fakayode, M. A. Busch, D. J. Bellert, and K. W. Busch, *Analyst* **130,** 233 (2005).

[62] S. O. Fakayode, M. A. Busch, and K. W. Busch, *Talanta* **68,** 1574 (2006).

[63] S. O. Fakayode, A. A. Williams, M. A. Busch, K. W. Busch, and I. M. Warner, *Journal of Fluorescence* **16,** 659 (2006).

[64] C. D. Tran, and D. Oliveira, *Analytical Biochemistry* **356,** 51 (2006).

[65] A. T. R. Williams, S. A. Winfield, and J. N. Miller, *Analyst* **108,** 1067 (1983).

[66] E. P. Kirby, and R. F. Steiner, *Journal of Physical Chemistry***,** 4480 (1970).

[67] A. E. Awrich, W. J. Stackhouse, J. E. Cantrell, J. H. Patterson, and D. Rudman, *Journal of Pediatrics* **87,** 731 (1975).

[68] O. Simell, J. Perheentupa, J. Rapola, J. K. Visakorpi, and L. E. Eskelin, *American Journal of Medicine* **59,** 229 (1975).

[69] N. W. Flodin, *Journal of the American College of Nutrition* **16,** 7 (1997).

[70] S. O. Fakayode, I. M. Swamidoss, M. A. Busch, and K. W. Busch, *Talanta* **65,** 838 (2005).

APPENDIX A

PLOT OF INTENSITY VERSUS ABSORBANCE OF CHIRAL MACROCYCLE AND L-TRP

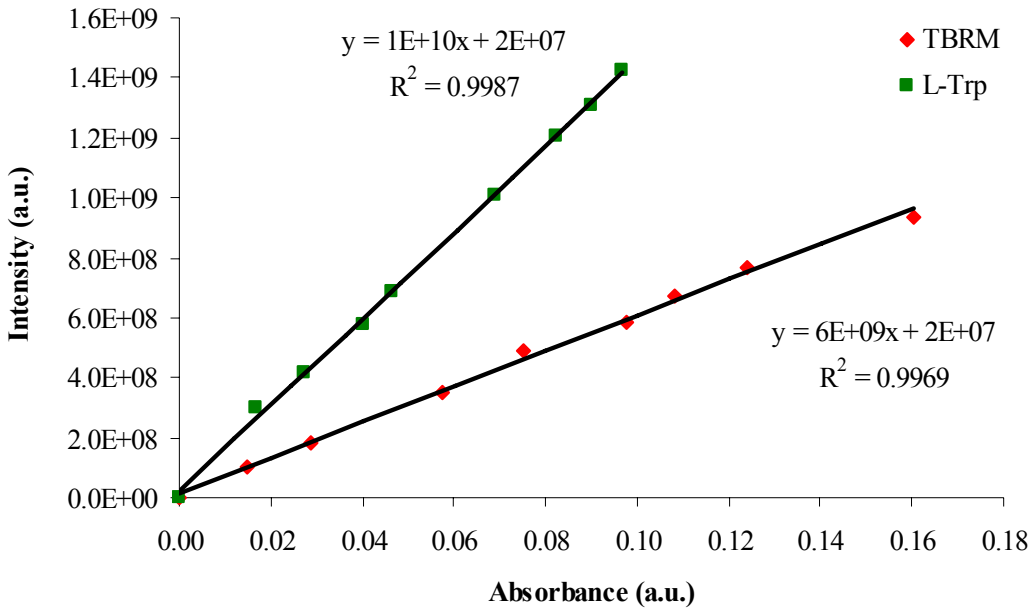

APPENDIX B

PLOT OF MOLAR ABSORPTIVITY VERSUS WAVELENGTH FOR CHIRAL MACROCYCLE

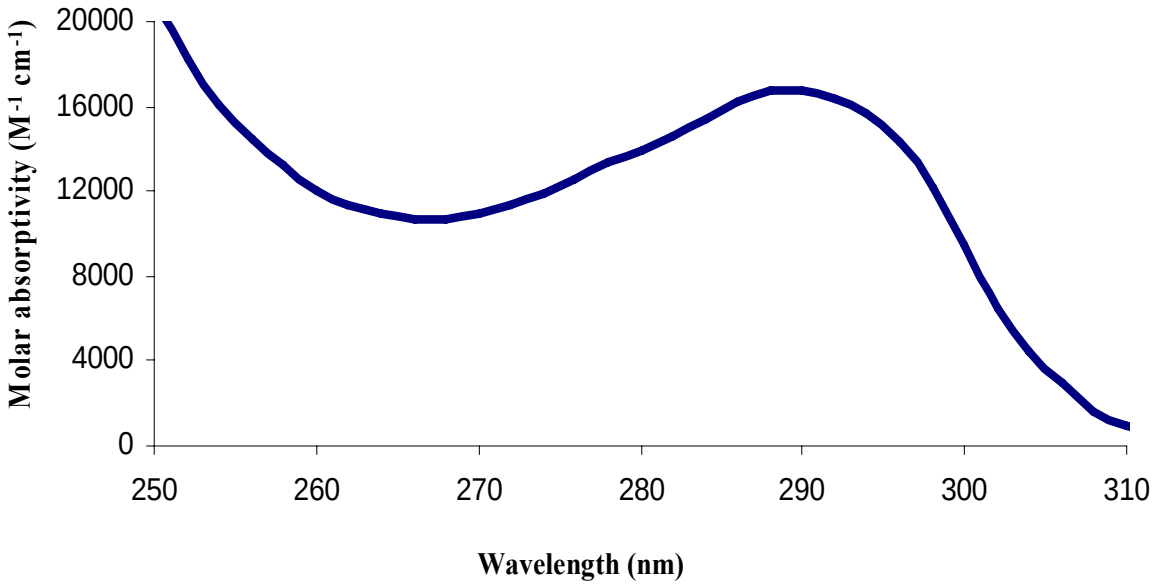

VITA

Gerald Richard obtained a bachelor of science in biochemistry, with honors, from Xavier University of Louisiana in May 2002. He is currently a master's degree candidate in the department of chemistry at Louisiana State University.